Research article

Dmitry A. Bykov[a], Evgeni A. Bezus[a,*] and Leonid L. Doskolovich

Bound states in the continuum and strong phase resonances in integrated Gires-Tournois interferometer

https://doi.org/10.1515/nanoph-2019-0316
Received August 13, 2019; revised November 20, 2019; accepted December 9, 2019

Abstract: Photonic bound states in the continuum (BICs) are eigenmodes with an infinite lifetime, which coexist with a continuous spectrum of radiating waves. BICs are not only of great theoretical interest but also have a wide range of practical applications, e.g. in the design of optical resonators. Here, we study this phenomenon in a new integrated nanophotonic element consisting of a single dielectric ridge terminating an abruptly ended slab waveguide. This structure can be considered as an on-chip analog of the Gires-Tournois interferometer (GTI). We demonstrate that the proposed integrated structure supports high-Q phase resonances and robust BICs. We develop a simple but extremely accurate coupled-wave model that clarifies the physics of BIC formation and enables predicting BIC locations. The developed model shows that the studied BICs are topologically protected and describes the strong phase resonance effect that occurs when two BICs with opposite topological charges annihilate.

Keywords: bound states in the continuum; resonance; mode coupling; integrated optics.

[a]**Dmitry A. Bykov and Evgeni A. Bezus:** These authors contributed equally to this work.
***Corresponding author: Evgeni A. Bezus,** Image Processing Systems Institute – Branch of the Federal Scientific Research Centre "Crystallography and Photonics" of Russian Academy of Sciences, 151 Molodogvardeyskaya St., Samara 443001, Russia; and Samara National Research University, 34 Moskovskoye Shosse, Samara 443086, Russia, e-mail: evgeni.bezus@gmail.com. https://orcid.org/0000-0002-9576-2360
Dmitry A. Bykov and Leonid L. Doskolovich: Image Processing Systems Institute – Branch of the Federal Scientific Research Centre "Crystallography and Photonics" of Russian Academy of Sciences, 151 Molodogvardeyskaya St., Samara 443001, Russia; and Samara National Research University, 34 Moskovskoye Shosse, Samara 443086, Russia

1 Introduction

Resonances are a key concept in photonics since they lie behind many intriguing optical effects arising in various photonic structures. Resonances occur when an eigenmode of the structure is excited, which is manifested in pronounced peaks in the transmittance and reflectance spectra and leads to local field enhancement, giving rise to extraordinary magneto-optical, nonlinear, and other optical effects. This makes resonant structures an indispensable building block for a wide range of photonic devices. High-Q resonators are particularly important in the design of lasers, filters, and sensors.

In the last decade, a fascinating phenomenon, which allows one to engineer resonances with an arbitrarily high quality factor, drew a lot of interest in photonics [1–4]. This phenomenon, referred to as bound states in the continuum (BICs), was first predicted for an electronic system by von Neumann and Wigner in 1929 [5]. In photonics, BICs are nonradiating eigenmodes of structures having open scattering channels. The leakage of the BIC energy into these channels is prevented by different mechanisms [3], including symmetry protection [6–8], interaction of several resonators [1, 9], and interference of several resonances in the same cavity [8, 10–16]. BICs have infinite quality factor, but a slight deviation from a BIC allows one to obtain resonances with extremely high-Q factors.

Different photonic structures have been shown to support BICs [3, 4]. Most studies on BICs are dedicated to periodic structures, in particular, photonic crystal slabs [1, 7, 12, 17–19], guided-mode resonant gratings [8, 15, 20], interfaces of photonic crystals [21], and infinite arrays of dielectric rods or spheres [19, 22–24]. In all these structures, the open scattering channels are the "free-space" diffraction orders. In Refs. [16, 25], the scattering channels are the waves propagating in anisotropic materials. In Refs. [2, 13, 14, 26–31], a different class of structures was studied, with the scattering channels being the modes of photonic crystal waveguides [2, 26–28], slab waveguides [13, 14, 29–31], or rectangular microwave waveguides [11].

Concerning the number of open scattering channels, most of the existing studies on BICs consider structures with two channels (reflected and transmitted); however, in Refs. [16, 21], the authors investigate BICs supported by structures with only one (reflected) channel open.

It was recently shown that BICs can be endowed with a topological invariant – topological charge, which takes integer values and is conserved upon the variation of the parameters of the structure [32]. BICs having nonzero topological charge are robust to these variations. Besides, the topological charge conservation law determines the possible interaction scenarios of several BICs [20, 24, 32, 33].

In this paper, we propose a new on-chip photonic structure – the integrated Gires-Tournois interferometer (GTI), which consists of a single dielectric ridge terminating an abruptly ended slab waveguide and operates in the total internal reflection geometry (i.e. it has a single open scattering channel). We demonstrate that, in contrast to its conventional (nonplanar) counterpart [34], the proposed integrated GTI supports high-Q phase-only resonances associated with the excitation of leaky eigenmodes of the ridge. Moreover, we show that these modes can accidentally decouple from the radiation continuum of the guided modes supported by the slab waveguide, which results in the formation of BICs. To the best of our knowledge, integrated structures supporting BICs associated with phase-only resonances have not yet been investigated despite their important potential applications in dispersion engineering, pulse compression, and phase encoding [34–36]. We present a simple and accurate analytical model that describes the optical properties of the studied integrated structure and reveals the mechanism behind BIC formation. By introducing the topological charge of the BICs, we prove that they are robust in the considered parameter space. Moreover, we show that the considered structure supports BICs only when the the coupling between the TE and TM guided modes at the second edge of the ridge is relatively weak. We formulate this "weak polarization coupling" condition analytically and show that when the structure is altered so that this condition becomes violated, BICs having opposite topological charges group in pairs, coalesce, and annihilate each other, leading to the strong phase resonance effect.

2 Integrated Gires-Tournois interferometer

First, let us recall the conventional GTI, which dates back to 1964 [34]. This interferometer (etalon) consists of a dielectric slab with the first interface being partially reflective and the second one having unit reflectivity (see the inset to Figure 1). Similar to the Fabry-Pérot interferometer, GTI exhibits resonant optical properties as a result of multiple reflections between the interfaces of the slab. If there is no absorption inside the GTI, the intensity of the reflected light is always unity, whereas its phase changes in a resonant manner. This makes GTI extremely important for various applications including dispersion compensation and compression of frequency-modulated light pulses [34–36].

Let us consider an integrated analog of the GTI, which is shown in Figure 1. The proposed structure consists of a single dielectric ridge with thickness h_r and width w terminating an abruptly ended slab waveguide with thickness h_a ($h_a < h_r$). We restrict our consideration to the case where both the slab waveguides with thicknesses h_a and h_r support only the fundamental TE- and TM-polarized guided modes. However, the effects discussed below can also occur in thicker multimode waveguides.

We study the diffraction of the TE-polarized guided mode obliquely incident from region A at the angle of incidence θ (Figure 1). We consider the monochromatic case with the time dependence $\exp(-i\omega t)$, where $\omega = 2\pi c/\lambda$ is the angular frequency and λ is the free-space wavelength of the incident light. The incident guided mode has a plane wavefront with the x-y dependence $\exp(ik_x x + ik_y y)$, where

$$k_x = k_0 n_{\mathrm{TE,inc}} \cos\theta, \quad k_y = k_0 n_{\mathrm{TE,inc}} \sin\theta \tag{1}$$

are the wave vector components. Here, $k_0 = 2\pi/\lambda$ is the wavenumber, and $n_{\mathrm{TE,inc}}$ is the effective refractive index of

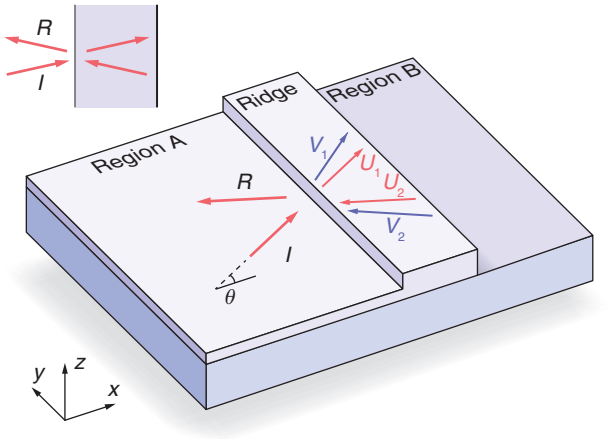

Figure 1: Geometry of the integrated Gires-Tournois interferometer (the structure is translation-invariant in the y-direction).
The arrows depict the propagation directions of the slab waveguide modes inside the structure. Red arrows show TE-polarized modes and blue arrows show TM-polarized modes. The inset shows the conventional GTI.

the incident TE-polarized guided mode (Figure 1). In some works, such waves are referred to as "semiguided planar waves" [37, 38].

At small angles of incidence, the outgoing field includes not only the reflected TE- and TM-polarized guided modes but also a continuum of propagating waves scattered out of the waveguide core layer. However, at relatively large angles of incidence, all these "parasitic" nonguided waves become evanescent and do not carry energy. We present a brief discussion of this scattering cancellation mechanism in the Supplementary Material section; several integrated nanophotonic elements exploiting this mechanism have been proposed recently [13, 14, 37–39].

Since there is no waveguide in region B (see Figure 1) and no out-of-plane scattering, all the energy is reflected at the second edge of the ridge and eventually returns to region A. Therefore, the structure works in the total internal reflection geometry. Moreover, if $n_{\mathrm{TE,inc}} \sin\theta > n_{\mathrm{TM,inc}}$, where $n_{\mathrm{TM,inc}}$ is the effective refractive index of the TM-polarized guided mode in region A, the reflected field contains only the TE-polarized mode, which has the same intensity as the incident wave. Therefore, the proposed integrated structure, similar to [16, 21], has only one open scattering channel.

In this regime, the structure indeed turns out to be an integrated analog of the GTI: the first interface of the ridge acts as a "weak" front mirror, whereas the second interface corresponds to a back mirror with unit reflectivity. Thus, the ridge itself can be considered as an interferometer cavity. There is, however, an important difference between the investigated on-chip structure and the conventional GTI. Indeed, at angles of incidence θ satisfying the inequality

$$n_{\mathrm{TM}} > n_{\mathrm{TE,inc}} \sin\theta > n_{\mathrm{TM,inc}}, \tag{2}$$

where n_{TM} is the effective refractive index of the TM-polarized mode in the ridge region, the outgoing field, as discussed above, consists of a single wave (the reflected TE mode), whereas in the ridge region, *two* different waves (the TE- and TM-polarized modes) propagate. This makes the proposed integrated structure somewhat similar to the recently investigated anisotropic layered structure [16].

In the rest of the article, we focus on the angle of incidence range defined by Eq. (2) and show that in this angular range the structure possesses remarkable resonant optical properties. To illustrate these properties, we consider an example with the following parameters: free-space wavelength $\lambda = 630$ nm; refractive indices of the superstrate, waveguide core layer, and substrate $n_{\mathrm{sup}} = 1$, $n_{\mathrm{inc}} = 3.32$ (GaP), and $n_{\mathrm{sub}} = 1.45$, respectively; and the waveguide thicknesses in region A and in the ridge region $h_a = 90$ nm and $h_r = 110$ nm, respectively. We emphasize that the used parameter values are not unique (no optimization of the structure was performed) and that the effects described below can be observed for a wide range of materials and waveguide thicknesses.

For the example under study, the slab waveguide in region A supports a TE-polarized mode with effective refractive index $n_{\mathrm{TE,inc}} = 2.681$ and a TM-polarized mode with effective refractive index $n_{\mathrm{TM,inc}} = 1.796$. The slab waveguide with thickness h_r corresponding to the ridge region supports TE- and TM-polarized modes with effective refractive indices $n_{\mathrm{TE}} = 2.819$ and $n_{\mathrm{TM}} = 2.187$, respectively. At these parameters, the inequality (2) is satisfied in the following angle of incidence range: $42.05° < \theta < 54.64°$.

Since the reflected TE-polarized mode has a constant (unit) amplitude in the angular range of interest, it is the phase of the reflected radiation that has to be investigated. The rigorously calculated dependence of the phase $\arg R$ on the ridge width w and the angle of incidence θ is shown in Figure 2A. The plot was arrived at using an efficient in-house implementation of the aperiodic Fourier modal method (AFMM), an established numerical technique for solving Maxwell's equations in integrated optics problems [40–42].

Figure 2A demonstrates that along with the smooth fringes caused by Fabry-Pérot resonances of TE-polarized guided modes in the ridge region, sharp resonant features are also present in the phase spectrum. The calculation of $\arg R$ in a wider angular range (not presented here) shows that the high-Q resonances occur only at the angles of incidence considered in Figure 2. As discussed above, at these angles the reflected radiation contains only the TE-polarized guided mode, whereas in the ridge region both the TE- and TM-polarized modes exist. The fact that the high-Q resonance region is located between the cut-off angles of the TM modes outside and inside the ridge suggests that these sharp features arise as a result of the excitation of cross-polarized (quasi-TM) eigenmodes of the ridge.

However, the most interesting feature of Figure 2A is that the width and, consequently, the quality factor of the phase resonances strongly vary along the dispersion curves. At the points marked with magenta circles, the resonances vanish, i.e. their widths turn to zero and their quality factors diverge. This is demonstrated by the rigorously calculated [13, 43, 44] Q-factor plot shown with a blue line in the inset to Figure 2A, which indicates the presence of BICs in the considered structure. Let us note that absorption, which is inevitable in realistic structures, turns infinite-Q BICs into high-Q resonances, referred to as quasi-BICs (see the red line in the inset to Figure 2A).

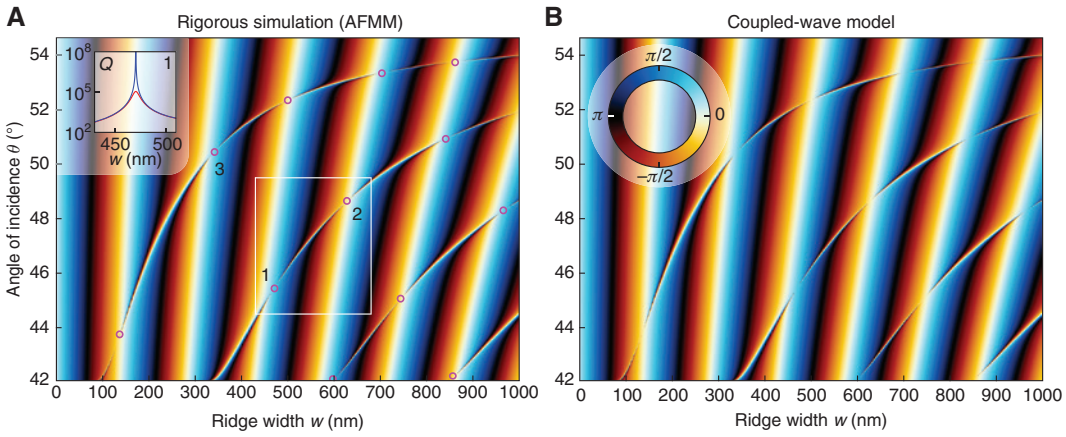

Figure 2: Phase of the reflected TE-polarized mode (arg R) vs. ridge width w and angle of incidence θ calculated using (A) AFMM and (B) the proposed coupled-wave model. Magenta circles show the BIC positions predicted using the coupled-wave model. The inset in (A) shows the quality factor of the resonance near the BIC marked with "1" (blue line); red line illustrates the decrease in the Q factor in the case when a small imaginary part ($k=10^{-5}$) is added to the refractive index of the waveguide. The BICs "1" and "2" bounded by the white rectangle are investigated in detail in Section 5.

Simulation results presented in the Supplementary Material section suggest that quality factor of the order k^{-1} can be achieved at quasi-BICs, where k is the extinction coefficient of the waveguide material. In addition, in the presence of absorption, the resonances are manifested not only in the phase of the reflected light but also as narrow dips in the reflection coefficient. As we demonstrate in the Supplementary Material section, the reflectance can almost vanish near quasi-BICs in lossy structures, which makes the considered structure promising for sensing applications [45].

Figure 3A shows the cross-sections of Figure 2A in the vicinity of the BIC marked with "3". The resonances in this plot are manifested in an arctangent-shaped rapid change of the phase. The angular widths of the resonances decrease when approaching the BIC condition. Similarly, the upper panel of Figure 3B, which shows the wavelength dependence of the phase arg $R(\lambda)$, also contains resonant features narrowing to zero when approaching the BIC. The presented plots suggest that the proposed integrated GTI can be used as a narrowband all-pass filter for transforming optical pulses and beams. The lower panel of Figure 3B shows the group delay $-\mathrm{d}\arg R/\mathrm{d}\omega$ introduced by the ridge structure (note the log scale used for the vertical axis). The group delay plots exhibit sharp resonant peaks, which are characteristic of GTIs [34]. Note that the peaks provided by conventional GTIs are evenly spaced with respect to the frequency, whereas in the considered integrated structure, we can obtain a single group delay peak on a wide, constant background. Moreover, when approaching the BIC, the maximum group delay increases by orders of magnitude (see the lower panel of Figure 3B).

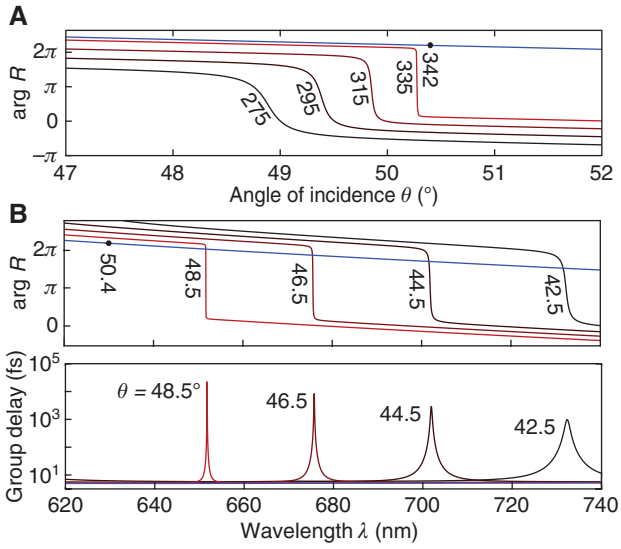

Figure 3: Phase of the reflected TE-polarized mode (arg R) vs. angle of incidence θ at different ridge widths $w=275$, 295, 315, 335, and 342 nm at $\lambda=630$ nm (A) and arg R (B, upper panel) and group delay (B, lower panel) vs. wavelength λ at different angles of incidence $\theta=42.5°$, 44.5°, 46.5°, 48.5°, and 50.4° at $w=342$ nm calculated using AFMM. The BIC condition is shown with black circles.

The maximum group delay ranges from ~1 ps at $\theta=42.5°$ to ~60 ps at $\theta=46.5°$. The width of the peaks is inversely proportional to the quality factor of the mode. For the considered parameters, the quality factor ranges from ~600 to ~47,000. In order to obtain such high-Q resonances using a conventional GTI with comparable thickness and materials, the reflectance at the first interface (see the inset to Figure 1) should be quite high: 0.98 (at $Q=600$) and 0.9997

(at $Q=47{,}000$). At the same time, the rest of the incident wave energy has to be transmitted (and not absorbed), which would normally require the use of multilayer dielectric structures. In the proposed integrated GTI, high-Q phase resonances are achieved using a different mechanism based on BICs.

In order to explain the BIC formation mechanism, in the following section we derive a simple but very accurate coupled-wave model, which proves the existence of BICs and enables predicting their locations in the parameter space.

3 Bound states in the continuum

In this section, we develop a coupled-wave model describing resonant optical properties of the considered structure and, in particular, BICs. The model is based on the fact that once we neglect the near-field effects, we can represent the field inside region A and inside the ridge region as a superposition of a small number of slab waveguide modes, which are coupled at the ridge edges.

As was shown in the previous section, the structure exhibits resonant properties when it has only one scattering channel, namely the reflected TE-polarized mode. We denote the complex amplitude of the wave corresponding to this channel by R and the amplitude of the incident wave by I. Inside the ridge region, there are both TE and TM slab waveguide modes with amplitudes $U_{1,2}$ and $V_{1,2}$, respectively. Here, the subscript "1" is used for the modes propagating from the first (left) edge of the ridge towards the second (right) one, and the subscript "2" denotes the modes that are reflected from the second edge and propagate backwards. The propagation directions of these six waves are schematically shown in Figure 1.

The considered modes are coupled at the edges of the ridge. The coupling at the first edge can be described by a 3×3 scattering matrix, which relates the complex amplitudes of the "scattered" modes (R, U_1, and V_1) with the amplitudes of the modes that are incident on the first edge of the ridge (I, U_2, and V_2):

$$\begin{bmatrix} R \\ U_1 \\ V_1 \end{bmatrix} = \underbrace{\begin{bmatrix} r & t_1 & t_2 \\ t_1 & r_1 & r_c \\ t_2 & r_c & r_2 \end{bmatrix}}_{\mathbf{S}_1} \begin{bmatrix} I \\ U_2 \\ V_2 \end{bmatrix}. \tag{3}$$

Here, r and t denote reflection and transmission coefficients, respectively. The subscripts denote the scattering channels being coupled: "1" and "2" correspond to the TE- and TM-polarized waves inside the ridge, whereas "c" corresponds to the cross-polarization coupling of the modes. Note that these coefficients depend on the angle of incidence θ and can be easily calculated using AFMM [40].

Similarly, the coupling at the second edge of the ridge is described by a 2×2 scattering matrix $\mathbf{S}_2$:

$$\begin{bmatrix} U_2 \mathrm{e}^{-\mathrm{i}\phi} \\ V_2 \mathrm{e}^{-\mathrm{i}\psi} \end{bmatrix} = \underbrace{\begin{bmatrix} q_1 & q_c \\ q_c & q_2 \end{bmatrix}}_{\mathbf{S}_2} \begin{bmatrix} U_1 \mathrm{e}^{\mathrm{i}\phi} \\ V_1 \mathrm{e}^{\mathrm{i}\psi} \end{bmatrix}, \tag{4}$$

where the subscripts have the same meaning as in Eq. (3). Since $U_{1,2}$ and $V_{1,2}$ denote the amplitudes of the modes at the first edge of the ridge, the scattering matrix $\mathbf{S}_2$ couples the amplitudes of the waves multiplied by the exponents describing the phase change acquired upon propagation of the modes between the ridge edges. The phases ϕ and ψ can be obtained by multiplying the wave vector components of the modes by the ridge width w:

$$\phi = k_x^{\mathrm{TE}} w, \quad \psi = k_x^{\mathrm{TM}} w, \tag{5}$$

where

$$(k_x^{\mathrm{TE}})^2 + k_y^2 = \left(\frac{\omega}{\mathrm{c}} n_{\mathrm{TE}}\right)^2, \; (k_x^{\mathrm{TM}})^2 + k_y^2 = \left(\frac{\omega}{\mathrm{c}} n_{\mathrm{TM}}\right)^2, \tag{6}$$

and k_y is defined in Eq. (1).

Equations (3) and (4) give a system of five coupled-wave equations describing the optical properties of the considered structure. In the Supplementary Material section, we solve these coupled-wave equations and obtain a closed-form expression for the reflection coefficient R. The obtained expression is quite complicated; however, since the considered structure is lossless, the scattering matrices $\mathbf{S}_1$ and $\mathbf{S}_2$ are unitary and it is possible to present the reflection coefficient in the following compact form:

$$R = \mathrm{e}^{2\mathrm{i}\phi} \mathrm{e}^{2\mathrm{i}\psi} d_1 d_2 \frac{\mathcal{D}^*}{\mathcal{D}}. \tag{7}$$

Here, $\mathcal{D}$ is the determinant of the matrix of the system of linear equations (3) and (4); $\mathcal{D}^*$ is the complex conjugate of $\mathcal{D}$; and $d_i = \det \mathbf{S}_i$, $i=1,2$, denote the scattering matrix determinants. Since the matrices $\mathbf{S}_1$ and $\mathbf{S}_2$ are unitary, $d_{1,2}$ have unit magnitudes, and, hence, the presented form of the reflection coefficient makes it obvious that $|R|=1$. The phase of the reflected light arg R, however, is not constant but changes resonantly when the eigenmodes of the structure are excited.

Figure 2B shows the phase of the reflected light (arg R) calculated using Eq. (7). By comparing Figure 2A and B, we see that the developed coupled-wave model is in excellent agreement with the full-wave simulation results. In particular, the presented model reproduces the sharp phase resonances with varying width, which are present in the rigorously calculated spectrum of Figure 2A.

The obtained Eq. (7) also makes it possible to prove BIC existence and allows one to calculate their positions in the parameter space. Since BICs are infinite-Q eigenmodes, the denominator $\mathcal{D}$ in Eq. (7) vanishes at a real frequency ω in the case of a BIC. This, however, does not lead to the divergence of R since the numerator in the case of a BIC vanishes as well [8, 13, 19]. In the Supplementary Material section, we present a rigorous proof of the fact that both the numerator and the denominator do indeed vanish at some real frequencies when the following constraint on the cross-polarization reflection coefficient q_c holds:

$$|q_c| \le \frac{2|t_1||t_2|}{|t_1|^2+|t_2|^2}. \tag{8}$$

According to this inequality, the considered structure supports BICs when q_c is relatively small. In particular, BICs always exist when no cross-polarization coupling occurs at the second edge of the ridge (at $q_c=0$). Therefore, BICs arise only in a certain part of the parameter space where the inequality (8), which can be called "weak polarization coupling" condition, is fulfilled. Let us note that inequality (8) is the cut-off condition for the BICs, which, however, is not related to the cut-off of any guided or scattered waves of the structure.

In the Supplementary Material section, we provide closed-form expressions for the phases ϕ and ψ satisfying the BIC condition. These phases, which are expressed in terms of the scattering matrices $\mathbf{S}_1$ and $\mathbf{S}_2$, are real when the inequality (8) holds. In this case, from Eqs. (5) and (6), we can find expressions for the ridge width w and the angle of incidence θ at which the structure supports a BIC:

$$w=\frac{c}{\omega}\sqrt{\frac{\phi^2-\psi^2}{n_{TE}^2-n_{TM}^2}},\ \theta=\arcsin\sqrt{\frac{n_{TM}^2\phi^2-n_{TE}^2\psi^2}{n_{TE,inc}^2(\phi^2-\psi^2)}}. \tag{9}$$

The BIC positions calculated using Eq. (9) and shown in Figure 2A are in perfect agreement with the features in the rigorously calculated phase of the reflected wave. Note that the positions of different BICs in Figure 2A were calculated by adding different integer multiples of 2π to the phases ϕ and ψ in Eq. (9). Similar equations can be obtained for the positions of the BICs in the ω-k_y parameter space.

4 Topological charge of the BICs

In this section, we demonstrate that BICs in the considered structure are topologically protected. We do this by showing that a nonzero integer topological charge can be assigned to each BIC. Usually, topological charge is defined as a curvilinear integral of some quantity calculated along a curve encircling a BIC in a certain parameter space [32]. Topological charge is introduced differently depending on the geometry of the structure. Approaches exploiting far-field polarization vector [32, 33] and argument of a quasimodal expansion coefficient [24] were recently proposed.

For the considered structure, we propose the following quantity to define the topological charge:

$$\mathcal{P}=d e^{i\phi}(q_c t_1^* e^{i\psi}-q_1 t_2^* e^{i\phi})-t_2, \tag{10}$$

which can be interpreted as the coupling coefficient between the incident light and the eigenmode of the integrated GTI (see Supplementary Material). To define the topological charge, we take the contour integral of the gradient of the argument of $\mathcal{P}$:

$$C=\frac{1}{2\pi}\oint_\gamma \mathrm{d}\arg\mathcal{P}(w,\theta), \tag{11}$$

where $\mathrm{d}\arg\mathcal{P}(w,\theta)=\frac{\partial\arg\mathcal{P}}{\partial w}\mathrm{d}w+\frac{\partial\arg\mathcal{P}}{\partial\theta}\mathrm{d}\theta$. We note here that the phases ϕ and ψ in $\mathcal{P}$ depend on both θ and w, whereas the coupling coefficients $q_{1,c}$ and $t_{1,2}$ depend solely on θ.

When the integration path γ encircles a BIC, Eq. (11) defines its topological charge. Moreover, when the topological charge is nonzero, there should be a point inside the integration contour where the phase of $\mathcal{P}$ is undefined. Therefore, at this point $\mathcal{P}=0$ and, as we prove in the Supplementary Material section, at this very point of the parameter space the considered structure supports a BIC.

Figure 4 shows arg $\mathcal{P}$ calculated in the considered w-θ parameter space. BICs are marked with white circles. One can see the singularities of arg $\mathcal{P}$ appearing at these points. Hence, if we move along a contour encircling a BIC, the phase will not return to its initial position but will differ by an integer multiple of 2π. For example, in the case of the BIC marked with "1" in Figure 4, the phase increases by 2π when encircling the BIC counterclockwise, and therefore its topological charge is +1. The phase around the BIC marked with "2", however, changes in the opposite direction, resulting in topological charge –1.

Small perturbations of the parameters of the structure result in small changes in the quantity $\mathcal{P}$. The integer

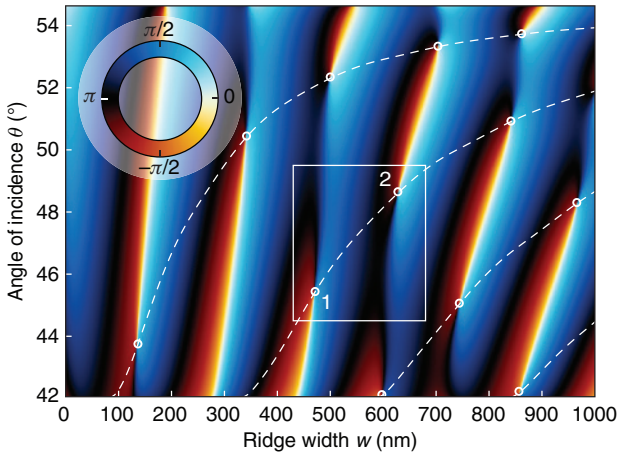

Figure 4: Phase of arg $\mathcal{P}$ vs. ridge width w and angle of incidence θ. As a guide to the eyes, the dashed lines show the dispersion of the quasi-TM modes of the ridge. White circles show the BIC positions predicted by the coupled-wave model.

value of the topological charge C, however, can only change in a discrete manner. Therefore, small perturbations will not change the topological charge and the BIC will not disappear but move in the parameter space. Such BICs are called "robust" or "topologically protected". Calculations based on Eq. (11) show that all the BICs investigated in this paper have nonzero topological charge and are, hence, robust.

Another important application of the topological charge is the investigation of the interaction of several BICs. To do this, let us choose the integration contour γ in such a way that it encircles several BICs. In this case, the value of C in Eq. (11) will be the sum of the topological charges of the encircled BIC. If the BICs interact in some manner, after the interaction the sum of the topological charges is conserved. One scenario for such an interaction is the annihilation of the BICs having opposite charges, which is discussed in the following section.

5 Annihilation of the BICs and strong phase resonances

As we have shown in the previous section, adjacent BICs in the considered structure have opposite topological charges (–1 and +1). The total topological charge of the two BICs is zero. Therefore, according to the charge conservation law, the coalescence of these BICs may result in their annihilation, after which no BICs remain, resulting in the same total charge equal to zero. In this section we demonstrate this effect.

To "move" the BICs in the parameter space, we introduce a nonzero thickness h_b of the waveguide layer in region B (see the inset to Figure 5B). We will assume that h_b is small enough so that the scattering channels corresponding to the transmitted modes in region B remain closed. In this case, the scattering matrix $\mathbf{S}_2$ changes but the coupled-wave model of Section 3 remains applicable.

Let us focus on the two BICs bounded by the white rectangle in Figure 2A. In the upper panels of Figure 5, we show the phase of the reflected wave calculated at different values of h_b ranging from 0 to 25 nm. The lower panels of Figure 5 show the corresponding rigorously calculated [43] quality factors of the modes. Note that the upper panel of Figure 5A is simply a magnified

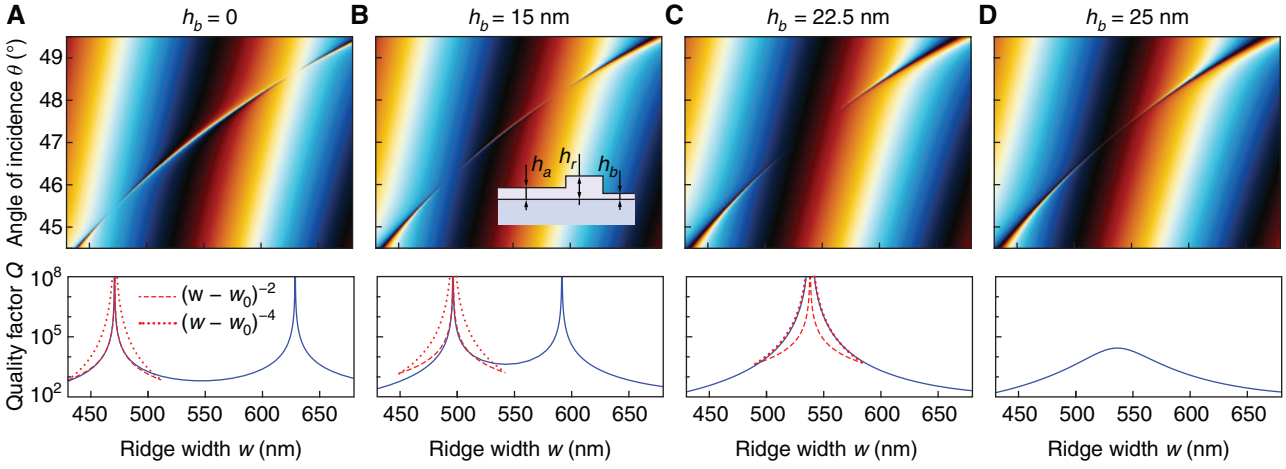

Figure 5: Phase of the reflected wave arg R (upper panels) and the corresponding quality factor of the resonance (lower panels) at (A) $h_b = 0$, (B) $h_b = 15$ nm, (C) $h_b = 22.5$ nm, and (D) $h_b = 25$ nm. Red lines show the fitting of the curves $(w - w_0)^{-2}$ (dashed lines) and $(w - w_0)^{-4}$ (dotted lines) to the calculated quality factor plots. The color map of Figure 2 is utilized.

fragment of Figure 2A, where two BICs are present. With an increase in h_b, these BICs approach each other (Figure 5B). Then, at a critical thickness $h_b = 22.5$ nm, the BICs coalesce, as shown in Figure 5C. At this thickness, the topological protection of the BIC is lifted, i.e. the considered "second-order" BIC in Figure 5C gets topological charge zero. If we further increase h_b, the BIC will disappear; indeed, instead of a BIC, only a finite-Q resonance is seen in Figure 5D corresponding to $h_b = 25$ nm. This demonstrates the annihilation of the BICs governed by their topological properties.

Now, let us focus on the lower panels of Figure 5 and investigate the w-dependence of the quality factor near the ridge width w_0 satisfying the BIC condition. To do this, we write the complex frequency of the mode ω_p in the big O notation: Re $\omega_p = \omega + O(w - w_0)$, Im $\omega_p = O((w - w_0)^2)$, which follows from the causality condition [19]. This expansion leads to a quadratic decay rate of the quality factor when moving away from the BIC: $Q = \text{Re}\ \omega_p/(-2\text{Im}\ \omega_p) \sim (w - w_0)^{-2}$. Indeed, in Figure 5A and B, the quadratic decay law $(w - w_0)^{-2}$ shown with dashed lines provides a good fit of the quality factor. However, this is not the case in Figure 5C, where the two BICs coalesce and the decay rate becomes quartic: $Q \sim (w - w_0)^{-4}$ (see the dotted lines in Figure 5). Note that a similar phenomenon was predicted for different periodic structures (photonic crystal slabs and arrays of cylinders or spheres) [20, 24, 33, 46, 47] and referred to as a *strong resonance* [24, 33, 46, 47]. Therefore, in the case of a "second-order" BIC, the proposed integrated GTI exhibits a strong *phase* resonance, which provides a slower decay of the quality factor when moving away from the BIC. This effect is of practical importance for designing high-Q resonators with relaxed fabrication tolerances.

Therefore, in this section we have shown that if the structure is altered in such a way that the weak polarization coupling condition (8) becomes violated, BICs having opposite topological charges group in pairs, coalesce, and, finally, annihilate each other.

6 Conclusion

In this work, we demonstrated that an integrated analog of the GTI, which consists of a single dielectric ridge terminating an abruptly ended slab waveguide, supports topologically protected BICs. We developed a coupled-wave model that accurately describes the resonant optical properties of the proposed structure. In particular, simple closed-form expressions were obtained for the condition of the BIC existence and for the positions of the BICs in the considered parameter space. The coupled-wave model also allowed us to introduce the topological charge of the BICs, proving their robustness and limiting their possible interaction scenarios by the charge conservation law.

The existence of BICs in the proposed structure makes it possible to use it as an integrated optical waveguide with an unconventional guiding mechanism [29–31]. Detuning from the BIC condition allows one to obtain an all-pass filter exhibiting sharp phase resonances. This makes the proposed structure promising for on-chip dispersion engineering, in particular for phase equalization and pulse compression. The existence of the so-called strong resonances in the considered structure relaxes the fabrication tolerances and makes the proposed integrated GTI an excellent candidate for creating high-Q optical resonators, which are widely used in filtering, sensing, and lasing. The latter application may fruitfully exploit the fact that the proposed structure has only one open scattering channel.

We believe that the proposed concept of an integrated GTI supporting BICs and strong phase resonances can be extended to other on-chip platforms, in particular Bloch surface waves propagating along the interfaces of photonic crystals [48]. We also expect that the demonstrated charge-conserving interaction of the BICs including their coalescence and annihilation can be implemented not only by changing the geometry of the structure but also through an external stimulus of magneto-optical, electro-optical, or nonlinear nature.

Acknowledgment: This work was funded by the Russian Foundation for Basic Research (Project No. 18-37-20038, Funder Id: http://dx.doi.org/10.13039/501100002261, coupled-wave model), the Russian Science Foundation (Project No. 19-19-00514, Funder Id: http://dx.doi.org/10.13039/501100006769, investigation of the topological properties of BICs), and the Ministry of Science and Higher Education of the Russian Federation (State assignment to the FSRC "Crystallography and Photonics" RAS under agreement 007-GZ/Ch3363/26, numerical simulations).

References

[1] Marinica DC, Borisov AG, Shabanov SV. Bound states in the continuum in photonics. Phys Rev Lett 2008;100:183902.
[2] Bulgakov EN, Sadreev AF. Bound states in the continuum in photonic waveguides inspired by defects. Phys Rev B 2008;78:075105.

[3] Hsu CW, Zhen B, Stone AD, Joannopoulos JD, Soljačić M. Bound states in the continuum. Nat Rev Mater 2016;1:16048.
[4] Koshelev K, Favraud G, Bogdanov A, Kivshar Y, Fratalocchi A. Nonradiating photonics with resonant dielectric nanostructures. Nanophotonics 2019;8:725–45.
[5] von Neumann J, Wigner E. Über merkwürdige diskrete eigenwerte. Phys Zeit 1929;30:467–70.
[6] Fan S, Joannopoulos JD. Analysis of guided resonances in photonic crystal slab. Phys Rev B 2002;65:235112.
[7] Shipman SP, Venakides S. Resonant transmission near nonrobust periodic slab modes. Phys Rev E 2005;71:026611.
[8] Bykov DA, Bezus EA, Doskolovich LL. Coupled-wave formalism for bound states in the continuum in guided-mode resonant gratings. Phys Rev A 2019;99:063805.
[9] Ndangali RF, Shabanov SV. Electromagnetic bound states in the radiation continuum for periodic double arrays of subwavelength dielectric cylinders. J Math Phys 2010;91:102901.
[10] Friedrich H, Wintgen D. Interfering resonances and bound states in the continuum. Phys Rev A 1985;32:3231–42.
[11] Lepetit T, Kanté B. Controlling multipolar radiation with symmetries for electromagnetic bound states in the continuum. Phys Rev B 2014;90:241103(R).
[12] Bulgakov EN, Maksimov DN. Avoided crossings and bound states in the continuum in low-contrast dielectric gratings. Phys Rev A 2018;98:053840.
[13] Bezus EA, Bykov DA, Doskolovich LL. Bound states in the continuum and high-Q resonances supported by a dielectric ridge on a slab waveguide. Photon Res 2018;6:1084–93.
[14] Nguyen TG, Ren G, Schoenhardt S, Knoerzer M, Boes A, Mitchell A. Ridge resonance in silicon photonics harnessing bound states in the continuum. Laser Photon Rev 2019;13:1900035.
[15] Bulgakov EN, Maksimov DN, Semina PN, Skorobogatov SA. Propagating bound states in the continuum in dielectric gratings. J Opt Soc Am B 2018;35:1218–22.
[16] Gomis-Bresco J, Artigas D, Torner L. Anisotropy-induced photonic bound states in the continuum. Nat Photon 2017;11:232–7.
[17] Hsu CW, Zhen B, Lee J, et al. Observation of trapped light within the radiation continuum. Nature 2013;499:188–91.
[18] Sadrieva ZF, Sinev IS, Koshelev KL, et al. Transition from optical bound states in the continuum to leaky resonances: role of substrate and roughness. ACS Photon 2017;4:723–7.
[19] Blanchard C, Hugonin J-P, Sauvan C. Fano resonances in photonic crystal slabs near optical bound states in the continuum. Phys Rev B 2016;94:155303.
[20] Jin J, Yin X, Ni L, Soljačić M, Zhen B, Peng C. Topologically enabled ultrahigh-Q guided resonances robust to out-of-plane scattering. Nature 2019;574:501–4.
[21] Hsu CW, Zhen B, Chua S-L, Johnson SG, Joannopoulos JD, Soljačić M. Bloch surface eigenstates within the radiation continuum. Light Sci Appl 2013;2:e84.
[22] Bulgakov EN, Sadreev AF. Bloch bound states in the radiation continuum in a periodic array of dielectric rods. Phys Rev A 2014;90:053801.
[23] Yuan L, Lu YY. Propagating Bloch modes above the lightline on a periodic array of cylinders. J Phys B 2017;50:05LT01.
[24] Bulgakov EN, Maksimov DN. Topological bound states in the continuum in arrays of dielectric spheres. Phys Rev Lett 2017;118:267401.
[25] Timofeev IV, Maksimov DN, Sadreev AF. Optical defect mode with tunable *q* factor in a one-dimensional anisotropic photonic crystal. Phys Rev B 2018;97:024306.
[26] Plotnik Y, Peleg O, Dreisow F, et al. Experimental observation of optical bound states in the continuum. Phys Rev Lett 2011;107:183901.
[27] Molina MI, Miroshnichenko AE, Kivshar YS. Surface bound states in the continuum. Phys Rev Lett 2012;108:070401.
[28] Weimann S, Xu Y, Keil R, et al. Compact surface Fano states embedded in the continuum of waveguide arrays. Phys Rev Lett 2013;111:240403.
[29] Zou CL, Cui JM, Sun FW, et al. Guiding light through optical bound states in the continuum for ultrahigh-Q microresonators. Laser Photon Rev 2015;9:114–9.
[30] Hope AP, Nguyen TG, Mitchell A, Bogaerts W. Quantitative analysis of TM lateral leakage in foundry fabricated silicon rib waveguides. IEEE Photon Technol Lett 2016;28:493–6.
[31] Yu Z, Xi X, Ma J, Tsang HK, Zou C-L, Sun X. Photonic integrated circuits with bound states in the continuum. Optica 2019;6:1342–8.
[32] Zhen B, Hsu CW, Lu L, Stone AD, Soljačić M. Topological nature of optical bound states in the continuum. Phys Rev Lett 2014;113:257401.
[33] Bulgakov EN, Maksimov DN. Bound states in the continuum and polarization singularities in periodic arrays of dielectric rods. Phys Rev A 2017;96:063833.
[34] Gires F, Tournois P. Interféromètre utilisable pour la compression d'impulsions lumineuses modulées en fréquence. C R Acad Sci Paris 1964;258:6112–5.
[35] Li KD, Knox WH, Pearson NM. Broadband cubic-phase compensation with resonant Gires–Tournois interferometers. Opt Lett 1989;14:450–2.
[36] Golubovic B, Austin RR, Steiner-Shepard MK, et al. Double Gires–Tournois interferometer negative-dispersion mirrors for use in tunable mode-locked lasers. Opt Lett 2000;25:275–7.
[37] Hammer M, Hildebrandt A, Förstner J. How planar optical waves can be made to climb dielectric steps. Opt Lett 2015;40:3711–4.
[38] Hammer M, Hildebrandt A, Förstner J. Full resonant transmission of semiguided planar waves through slab waveguide steps at oblique incidence. J Lightwave Technol 2016;34:997–1005.
[39] Doskolovich LL, Bezus EA, Bykov DA. Two-groove narrowband transmission filter integrated into a slab waveguide. Photon Res 2018;6:61–5.
[40] Silberstein E, Lalanne P, Hugonin J-P, Cao Q. Use of grating theories in integrated optics. J Opt Soc Am A 2001;18:2865–75.
[41] Li L. Formulation and comparison of two recursive matrix algorithms for modeling layered diffraction gratings. J Opt Soc Am A 1996;13:1024–35.
[42] Hugonin JP, Lalanne P. Perfectly matched layers as nonlinear coordinate transforms: a generalized formalization. J Opt Soc Am A 2005;22:1844–9.
[43] Bykov DA, Doskolovich LL. On the use of the Fourier modal method for calculation of localized eigenmodes of integrated optical resonators. Computer Opt 2015;39:663–73.
[44] Bykov DA, Doskolovich LL. Numerical methods for calculating poles of the scattering matrix with applications in grating theory. J Lightwave Technol 2013;31:793–801.
[45] Nesterenko DV, Hayashi S, Sekkat Z. Extremely narrow resonances, giant sensitivity and field enhancement in low-loss waveguide sensors. J Opt 2016;18:065004.

[46] Yuan L, Lu YY. Strong resonances on periodic arrays of cylinders and optical bistability with weak incident waves. Phys Rev A 2017;95:023834.
[47] Yuan L, Lu YY. Bound states in the continuum on periodic structures surrounded by strong resonances. Phys Rev A 2018;97:043828.
[48] Vinogradov AP, Dorofeenko AV, Merzlikin AM, Lisyansky AA. Surface states in photonic crystals. Phys–Usp 2010;53:243–56.

Supplementary Material: The online version of this article offers supplementary material (https://doi.org/10.1515/nanoph-2019-0316).